Effect of the low-frequency turbulence on the aeroelastic response of a long-span bridge in wind tunnel

Tommaso Argentini[a,*], Daniele Rocchi[a], Claudio Somaschini[a]

[a] Politecnico di Milano, Department of Mechanical Engineering, via La Masa 1, 20156 Milano, Italy

Abstract

The influence of the low frequency turbulence components on the buffeting response of long span bridges was studied through experimental tests performed on a full bridge aeroelastic model in the wind tunnel of the Politecnico di Milano, using an active turbulence generator producing a correlated deterministic harmonic turbulence. The experimental evidence underlined the nonlinear effect of the low frequency incoming turbulence on the dynamic resonant response of the structure at higher frequencies.

Numerical simulations are used to explain the bridge behavior considering the variation of the aeroelastic properties of the bridge with the instantaneous angle of attack and reduced velocity. Even though wind tunnel experiment uses an oversimplified wind spectrum with an intentionally high correlation along the main span, it helps to understand the nonlinear interaction between the low frequency and the high frequency buffeting response on a full bridge.

Key words:
wind tunnel, aeroelastic model, long span bridge, band superposition, buffeting, aeroelasticity

1. Introduction

In bridges aerodynamics, modeling the non-linearities of wind loads acting on decks is still an open issue. International research groups started recently to compare the results of the most widely used numerical approaches in long span bridge design (Diana et al., 2019a,b) to compute the aeroelastic response of the structure. Most of these approaches

*Corresponding author
Email address: tommaso.argentini@polimi.it (Tommaso Argentini)

rely on linearized numerical models to compute the aerodynamic forces acting on bridge elements (mainly the deck), considering small variation of the relative angle of attack between incoming wind and bridge deck around the static position taken by the structure under the action of mean wind speed.

While this linearization hypothesis is valid when the contribution of the deck rotation to the variation of the instantaneous angle of attack is considered (a good aerodynamic design aims to small vibrations), large variations of angle of attack can be anyhow produced by the turbulent fluctuations of the incoming wind velocity. This consideration is widely agreed in bridge aerodynamics and it is supported by full scale measurements (e.g. Fenerci and Øiseth (2018); Bocciolone et al. (1992); Hui et al. (2009)). Modern full-scale experimental techniques (e.g. LIDARS, see Cheynet et al. (2017a,b); Mikkelsen et al. (2017)), adopted in recent full scale monitoring, allow today to better investigate the characteristics of the real wind blowing on long span bridges confirming the presence of large variation of the vertical component of the wind velocity and thus of the instantaneous angle of attack on the deck.

Looking at the spectrum of the turbulent incoming wind and to the physics of the Atmospheric Boundary Layer, the largest variations of the turbulent wind velocity components are due to low frequency contributions of the large scale eddies and this consideration is at the base of numerical methods to compute bridge buffeting response called "Band superposition" methods (Diana et al., 1995; Chen and Kareem, 2001). These approaches aim at reproducing with different numerical modeling the "Low Frequency" (LF) and the "High Frequency" (HF) part of the aeroelastic response. The adoption of different numerical models to compute the aerodynamic forces in the two frequency ranges is based on the assumption that the aerodynamic forces dependency on reduced velocity (V^*) is weak at LF, where large variations of the instantaneous angle of attack occur, while it is stronger at HF where the variation of the instantaneous angle of attack is small.

Quasi-Steady Theory approaches (Diana et al., 1995; Chen and Kareem, 2001) proved to be effective numerical models to reproduce the aerodynamic forces dependency on the angle of attack when V^* dependency is weak and they are used to compute the LF part of the aeroelastic response. Usually the angle of attack dependency is strongly nonlinear for the drag force for all the bridge deck typologies and it is increasingly nonlinear also for the lift force and for the aerodynamic moment, in particular if multi-box deck sections are considered (Diana et al., 2008). Simulation of the HF range is performed separately from the LF range using conventional linear methods based on flutter derivatives and admittance functions in time domain where aerodynamic coefficients are updated at each time step using the instantaneous LF angle of attack.

Time domain models are required to model the interaction between the LF and HF aeroelastic response since the LF variation of the angle of attack is time dependent. Taking into account the large V^* dependency in the HF range, this is a challenging task for time domain models and research is still active on this topic. Volterra series methods (Wu and Kareem, 2014; Carassale et al., 2014) and rheological models (Diana et al., 2013a) are two recent approaches to deal with this problem. An application of these methods in the full range of V^* and angle of attack is limited by the need of specific experimental wind tunnel tests to identify the numerical model parameters.

Rheological models identification for instance is based on aerodynamic hysteresis loops and the model is proposed to overcome Quasi Steady Theory limitation and to try to model the dependency of the aerodynamic forces upon both angle of attack and reduced velocity in the LF and HF range (Diana et al., 2010, 2013a).

Independently from the applied numerical modeling, Band-Superposition methods are today more used in research than in practical bridge design where LF-HF interaction is usually neglected. Nevertheless the evolution of long span bridges towards more complex aerodynamic solutions (longer spans, multi-box decks, environmental effects,..) and the availability of more performing experimental facilities and larger computation power help to better investigate the aeroelastic problem and the interaction between LF and HF contributions and to develop better numerical models to take into account these effects also on conventional bridge solutions like the one investigated in this paper.

At present, investigations on LF and HF range interaction are usually performed by means of wind tunnel tests on sectional deck models using turbulence active generation with both forced motion or elastically suspended set-ups (Diana et al., 2010, 2013b; Ma et al., 2013) , and no evidence is present in literature on full aeroelastic models. In this paper, we present the experimental results of a wind tunnel campaign performed on an aeroelastic model of long span-bridge (1:220 scale) aimed at highlighting the effects of LF incoming turbulence on the dynamic HF response of the structure. To this end, an active turbulence generator was used to generate a correlated deterministic harmonic turbulence. The active turbulent generator is able to produce a multi-harmonic perturbation of the flow with a strongly correlated vertical component of the wind velocity.

The perturbation consists in the superposition of single harmonics in order to simplify the incoming turbulent wind. The usual wind tunnel tests performed on full bridge aeroelastic model with the passive reproduction of the whole turbulent wind spectrum does not allow to appreciate the non linear interaction since the contributions of all the harmonics is overlapped.

In this case, the response of the structure was recorded under two different incoming flow conditions:

a) HF turbulence component only;

b) superposition of HF and LF turbulence components.

Comparing the high frequency responses of the bridge in the two different cases, it is possible to highlight the interaction effects of the LF incoming turbulence that can be analyzed and explained using numerical models. Indeed, numerical simulations are performed in order to explain the different aeroelastic behavior of the bridge: initially an eigenvalue-eigenvectors analysis of the aeroelastic system is performed to show the effect of the dependence of aerodynamic forces on the angle of attack and reduced velocity. Furthermore, a Band Superposition simulation in time domain is performed to highlight the method capability to reproduce the strongly non-linear aeroelastic response.

2. Experimental setup

2.1. Aeroelastic model of the full bridge

The bridge studied in the present research is the Izmit Bay Bridge, a three spans suspension bridge with a main central span of 1550 m and two side spans of 566 m. Each tower is a 252 m high steel structure having two crossbeams connecting the two tower legs at the middle level and at the top. Towers foundations are placed on the gravel bed, at 40 m below the water level. Main cables are deviated at the side span piers and anchored at the cable anchor blocks. The bridge deck is a classical streamlined single box (with a three-lane dual carriageway with guardrails), 36.4 m wide and 4.75 m deep, having 2.8 m wide inspection walkway with parapets on both sides. The general arrangement of the bridge and the deck cross-section are shown in Figure 1. Aeroelastic tests were performed on an aeroelastic model of the full bridge in the Boundary Layer Wind Tunnel of Politecnico di Milano. The model was realized in a 1:220 geometrical scale, using Froude similarity (Diana et al., 2013b; Argentini et al., 2016).

2.2. Aerodynamic coefficients

Static aerodynamic coefficients and torsional flutter derivatives were measured for the deck. The aerodynamic static coefficients were measured on a sectional model, 1.5 m long, with the same geometrical scale of the full-bridge to match the Reynolds number of the aeroelastic tests. The sectional model was mounted inside two vertical flat plates to guarantee a bi-dimensional flow. Outside the flat plates, the model was supported by two six-axis force balances. Vertical and transverse motions were constrained, while the rotation was imposed on both sides by means of an electric motor.

Since large angles of attack were expected in the aeroelastic tests presented in this study, aerodynamic coefficients were measured as a function of a wide range of mean angles of attack α: static coefficients from -10 deg to +10 deg, with step 2 deg; flutter derivatives coefficients from -6 to +6 deg, with step 2 deg.

Considering the sign conventions reported in Figure 2, static drag, lift and moment, acting on the deck section per unit length, are defined as:

$$F_D = \frac{1}{2}\rho B U^2 C_D(\alpha) \tag{1}$$

$$F_L = \frac{1}{2}\rho B U^2 C_L(\alpha) \tag{2}$$

$$M = \frac{1}{2}\rho B^2 U^2 C_M(\alpha) \tag{3}$$

where $C_{D,L,M}$ are the static aerodynamic coefficients, ρ is air density, B is the deck chord, U is the mean wind speed, α is the angle of attack. The static force coefficients are reported in Figure 3a), and they have classical values and slopes of closed-box deck sections.

The self-excited lift and moment per unit length, acting on the deck, related to the torsional motion θ can be defined as (using the definition in (Zasso, 1996):

$$L_{se} = \frac{1}{2}\rho U^2 B \left(-h_2^* \frac{B\dot{\theta}}{U} + h_3^* \theta\right) \tag{4}$$

$$M_{se} = \frac{1}{2}\rho U^2 B^2 \left(-a_2^* \frac{B\dot{\theta}}{U} + a_3^* \theta\right) \tag{5}$$

where a_i^*, h_i^* are the flutter derivative coefficients , function of reduced velocity $V^* = \frac{U}{fB}$ (f frequency of motion) and mean angle of attack α.

Flutter derivatives were measured with the same setup and model, using a forced motion technique (Diana et al., 2004), and they are reported in Figure 3b), for the reduced velocity $V^* = 11.7$, as a function of the mean angle of attack. The reason why this specific reduced velocity is shown will be explained in the next Sections.

However, we can introduce a first comment about the value of a_2^* coefficient: using the definition in Eq.(5), $a_2^* > 0$ means positive torsional aerodynamic damping, while $a_2^* < 0$ means negative damping; looking at the values reported in Figure 3b), it is possible to notice that $a_2^* > 0.4$ for mean values of α in the range between -6 and +4 deg, while its value decreases to 0.1 for $\alpha = 6$ deg, therefore the aerodynamic damping is largely reduced if α exceeds +4 deg. This specific trend will be used to explain some experimental findings in the following Sections.

Vertical and horizontal unsteady aerodynamic coefficients were not measured, and, in the numerical simulations, their values were inferred from quasi-steady theory.

2.3. Active turbulence generator

An active turbulence generator, sketched in Figure 4, was used to generate harmonic wind waves (Diana et al., 2013a). The generator, 4 m wide and placed 7 m upwind the model, is composed by a vertical array of 10 NACA 0012 airfoils with a chord of 0.2 m each). All the airfoils were driven synchronously by two brushless motors giving a pitching motion according to a user-defined motion law in terms of frequency and amplitude. No atmospheric boundary layer is reproduced during the aeroelastic tests and the airfoils deflect the incoming smooth wind causing a 4 m wide coherent wave. This wave excite most of the main span of the bridge, whose length is 5 m, while the total length of the bridge is 12 m (Figure 4b)).

The flow was measured along the main span, one chord upwind the leading edge of the deck, by means of three 4-holes cobra probes, able to measure the instantaneous vertical and horizontal wind components.

By varying the frequency and amplitude of the airfoils oscillation, it is possible to study different turbulent wind conditions. In particular, it is possible to:

1. generate only LF fluctuations of w, that in turn generates LF variations of the wind angle β_{LF}. Consequently a LF fluctuation of the angle of attack $\alpha_{LF} = \beta_{LF} + \theta_{LF}$ (see Figure 2) forces quasi-steadily the bridge, being θ_{LF} the LF torsional response of the deck.
2. generate only HF fluctuations, usually forcing the bridge in resonance, in order to highlight the aeroelastic response.
3. generate both HF and LF fluctuations to check if the aeroelastic effects are linear and superposition principle holds, or if nonlinear effects are present and the HF response is influenced by the LF fluctuations.

A picture of the experimental setup is shown in Figure 5.

2.4. Bridge dynamic properties

Since the turbulence generator is placed in the middle of the main span, the vibration modes forced by the coherent fluctuations are mainly the symmetrical ones with respect to the center of the bridge.

During the wind tunnel test campaign also the flutter instability of the bridge was studied, resulting in a critical speed of 5.53 m/s and a flutter frequency of 2.57 Hz in model scale (full-scale: 82 m/s and 0.173 Hz),(Argentini et al., 2016).

The structural modes mainly involved in the flutter are the first and the fifth vertical bending and the first torsional one, named respectively 1V, 5V, and 1T. The experimental natural frequencies of these modes are 1.31 Hz, 2.87 Hz and 3.84 Hz respectively (full-scale: 0.0885 Hz, 0.1934 Hz, and 0.2592 Hz), and their mode-shapes (taken from a finite element model) are reported in Figure 6.

3. Experimental results

Two different wind tunnel tests were performed to investigate the effects of LF coherent fluctuations of the incoming turbulent wind on the HF aeroelastic response of the bridge:

Case a) : single-harmonic vertical turbulence component with a HF content at 2.57 Hz (reduced velocity $V^* = V/(fB) = 11.7$) and small amplitude (β_{HF}=1 deg), representing a simplified contribution of the high frequency part of the wind spectrum;

Case b) : double-harmonic vertical turbulence component with HF content at 2.57 Hz with small amplitude ($\beta_{HF} = 1$ deg) plus LF content at 0.1 Hz (reduced velocity $V^* = 303$) with amplitude $\beta_{LF} = 2$ deg, representing simplified simulation of the wind spectrum with frequency content both at LF and HF.

A mean wind speed of 5 m/s was chosen in both cases, in order to have a strong aerodynamic coupling between modes: indeed, the HF forcing at 2.57 Hz is a frequency near the torsional frequency of the aeroelastic model at a mean wind speed of 5 m/s.

3.1. Generated flow

The angles of attack for both cases, measured at deck height by the multi-hole probe at mid-span, are shown in Figure 7 in terms of spectra. In Case a), as expected, the flow is characterized by a constant horizontal mean velocity component with a vertical HF velocity component at 2.57 Hz. In Case b), the LF content is clearly visible, and in the HF some sub- and super- harmonics are present, probably due to floor effect. However, in the authors' opinion, this boundary effect can be neglected with regard to the results presented in this paper.

In the Supplementary data, the reader can find a video recorded during Case b) tests where it is possible to observe the two overlapped wavelengths of the LF and HF components in the active generator and their effect on the response the bridge.

3.2. Bridge aeroelastic response

Figure 8 shows the recorded vertical accelerations at mid-span, measured with on-board MEMS accelerometers, overlapped to the LF time history of the angle of attack for both cases. Comparing the time histories of the aeroelastic response (red lines) in Case b) with the one in Case a), it is possible to observe that the HF dynamic response is strongly dependent on the LF incoming turbulence.

In particular, at the maximum positive LF angles of attack generated by the incoming turbulence the deck response amplitude is more than twice the reference Case a). This result shows that, although in the two cases the mean speed and the HF contents are almost the same, the bridge reacts in two very different ways depending on the LF instantaneous angle of attack.

This behavior can be explained looking at the dependence of the unsteady aerodynamic coefficients upon the mean angle of attack. Considering that the static rotation of the deck is 2 degrees nose up at 5 m/s, the angle of attack in Case b) oscillates between -4 and 6 degrees (see Fig. 8b). On the other hand the mean wind speed is steady, this means that the reduced velocity does not change between the two cases, and it is possible to study the trend of the flutter derivatives as a function of the angle of attack, as shown in Figure 2b for $V^* = 11.7$.

The aerodynamic coefficients that are more influenced by the angle of attack are a_2^* and h_2^*. Specifically a_2^*, that is the coefficient related to the aerodynamic torsional damping, has a decreasing trend for positive angles of attack, and it reaches nearly 0 at +6 deg, as previously already commented. The larger dynamic response observed at $\alpha_{LF} > 4$ deg can be therefore related to the total damping of the bridge model (structural plus aerodynamic) due to the dependency of aerodynamic coefficients upon the angle of attack.

To support this hypothesis we have to suppose that the aerodynamic coefficients depends upon the LF angle of attack, and not only on the mean angle of attack. In the following section, different numerical models are used to support this explanation and to show the need to consider the effect of α_{LF} on the HF aeroelastic response.

4. Numerical results

Two different kind of numerical simulations were performed to study the experimental behavior: a simple eigenvalue-eigenvector analysis, and a more complex Band-Superposition analysis.

4.1. Eigenvalue-eigenvector analysis

Starting from the results of the experimental campaign, a numerical study was carried out in order to investigate the effect of different mean angles of attack on the aeroelastic coupling of the bridge, and specifically on its eigenvalues/eigenvectors. The used algorithm is based on multi-modal equations and it solves the eigenvalue problem at different wind speeds, considering smooth flow conditions (Argentini et al., 2014). The three symmetric modes reported in Figure 6 were used in the simulations since they are the most important modes for the symmetric flutter instability.

In Figure 9a), the computed numerical static rotation of the deck, as a function of the mean wind speed is shown: we can note that at 5 m/s the mean static rotation of the deck at midspan is $\theta_{ST} = 2$ deg.

In Figure 9b), the damping evolution of the 3-mode system (1V-5V-1T) is reported as a function of the wind speed; we consider smooth flow conditions, so the angle of attack α is the deck rotation θ_{ST}. We notice that the lowest damping at 5 m/s is the one of "1T" mode, with damping ratio value of about 0.04.

Starting from this case, other simulations were run, changing the value of the angle of attack by summing to θ_{ST} a value of +4, +2, -2, and -6 deg, and the obtained results are shown in Figure 10, in comparison with the reference case $\alpha = \theta_{ST}$.

On the one hand, it is clearly visible that the "1T" mode, at 5 m/s of wind speed and at angles of attack $\theta_{ST} - 6°$ and $\theta_{ST} - 2°$ has the same total damping ratio of the reference case ($\approx 4.5\%$). On the other hand, the simulation with $\theta_{ST}+2°$ shows a smaller damping ratio ($\approx 1\%$), while at $\theta_{ST} + 4°$ total damping is negative, meaning bridge in flutter instability. This means that the variation of the angle of attack, constant in these simulations and variable at LF in wind tunnel tests, might shift the eigenvalues of the system from a stable condition to a less stable, or even unstable, condition.

These simulations are not intended to compute the aeroelastic behavior for different static angles of attack, but to study what can occur when a β_{LF} produces an instantaneous angle of attack α_{LF}, slowly ranging from -4 to +6 deg, as in the experimental tests.

To be thorough, in Figure 11 the magnitudes and the phases of the eigenvectors at 5 m/s of the mode *1T* are shown for all these simulations. From the comparison, the eigenvectors are very similar, therefore we can confirm that the different total damping is linked to the direct aerodynamic damping a_2^* and not to a different coupling of the structural (no-wind) mode shapes.

4.2. Band Superposition simulation

The behavior of the bridge has also been simulated with a Band-Superposition model applied to the full bridge, in order to take into account the β_{LF}.

The Band Superposition procedure, which is here briefly summarized, consists of four main steps:

1. LF response computation
2. HF response computation

3. sum of LF and HF response

For the considered case, the LF vertical wind speed component is mono-harmonic at 0.1 Hz ($V^* = 303$) with amplitude $\beta = 2$ deg. The LF computation is simulated using a nonlinear corrected quasi-steady theory (e.g. Diana et al. (1995)).

The HF band solution can be simulated with a rheological numerical model (Diana et al., 2013a) or with a multi-band approach (Diana et al., 2005). Both approaches model HF forces with parameters that are modulated by the instantaneous LF angle of attack, α_{LF}: self-induced and buffeting forces are computed independently and their effect are summed up exploiting the superposition hypothesis around the low-frequency angle of attack. In the considered test (Case b)) the central part of the mid-span is forced by a turbulent vertical wind component at 2.57 Hz ($V^* = 11.7$) with amplitude $\beta_{HF} = 1$ deg, plus a $\beta_{LF} = 2$ deg at 0.1 Hz ($V^* = 303$), while the lateral spans are forced by a laminar wind.

For this forcing conditions, a multi-band model is used for the numerical simulations, because only a single reduced velocity is present in the high-frequency range and therefore it is easily implemented, since flutter derivatives are considered at a fixed reduced velocity and function only of α_{LF}. Figure 12 shows the comparison between the simulated and the experimental time history of the torsional acceleration at the mid-span section, and the time history of the experimental α_{LF}, β_{LF}, and θ_{LF}.

We can highlight that the main effects of the LF angle of attack is well reproduced: in particular, there is an amplification of the response for positive α_{LF}, and a reduction for negative α_{LF}; the dependency on the α_{LF} in the response is caught, even if the amplitude of the numerical response has some differences: in particular, it is larger for negative α_{LF}, but the maximum vibration levels, for the equivalent acceleration at deck edge, are in both cases about 3 m/s^2.

To analyze the differences in the experimental-numerical comparison, we should remember that the variation of α_{LF} lead to a variation of total damping between negative and positive values, according to results obtained at constant mean angle of attack. However, in this test case, the system is always in transient-state conditions and the aerodynamics could not be fully described by the flutter derivatives that represent a steady-state condition around a specific mean angle of attack: further investigations on this topic are suggested for future research studies.

5. Conclusions

The research presented in this paper provides a further contribution in the investigation of non-linear effects in the aeroelastic response of long span bridges.

The artificial over-simplified wind scenario composed by single harmonics in the vertical component of the incoming wind velocity acting with almost full spatial coherence on the central part of the full bridge aeroelastic model is intentionally used to study the interaction between LF and HF aeroelastic response of the structure. It is confirmed that the HF response of the bridge is modified by the large fluctuations of the angle of attack induced by the incoming wind.

A numerical analysis of the aeroelastic effects shows very well how the HF response is not only due to the aerodynamic force dependency on V^*, but also on their dependency on the instantaneous angle of attack.

Even for a very common deck section like the conventional single box deck section of the bridge considered in this study, large variation of the flutter derivatives aerodynamic coefficients occur, if different angle of attack are considered. Since the variation of the instantaneous angle of attack can be produced by the LF turbulent fluctuations of the incoming wind, aerodynamic forces can vary largely inducing non linear effects in the structural response.

Band superposition approaches can reproduce the observed aeroelastic behavior of the bridge under the condition to have the flutter derivatives coefficients for the required V^* range and for a large set of angles of attack. This is not a usual condition since flutter derivatives are commonly measured either only at a mean angle of attack equal to zero or in a small range of angles of attack around zero. For the considered case the maximum instantaneous angle of attack is for instance 6 deg.

Even if the wind spectrum was over-simplified, reproducing only two frequency components at LF and HF, and even if the spatial correlation is extremely large along the central span, the structural dynamics of the model and the aerodynamic coefficients of the deck are representative of real long span bridge. Therefore the dynamic response of the bridge is the result of both the aeroelastic coupling of structural modes and of the buffeting excitation.

This test-case is another evidence that supports the need for a characterization of the deck unsteady aerodynamics in a large range of angles of attack also at low reduced velocities. Further research should be devoted to extend this methodology to a full-spectrum incoming turbulent wind, to assess how low-frequency fluctuations of the wind affect the aeroelastic response of structures in the atmospheric boundary layer.

6. Figures

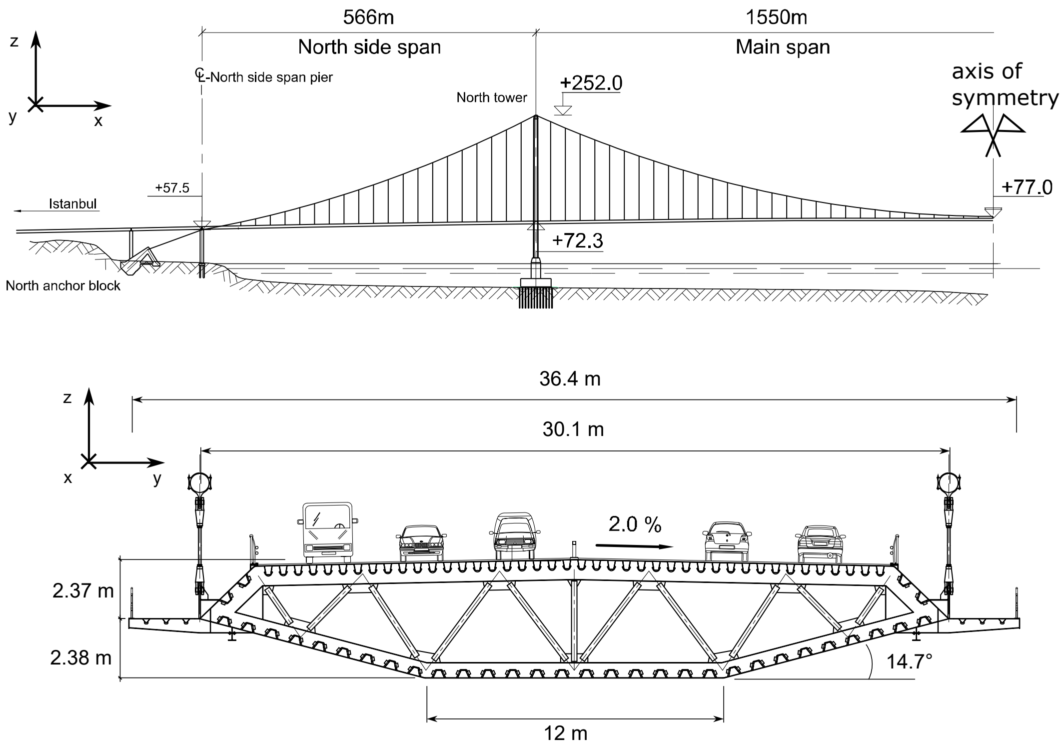

Figure 1: General arrangement of the bridge (the bridge is symmetric and only half of the complete bridge is shown) and typical deck cross-section

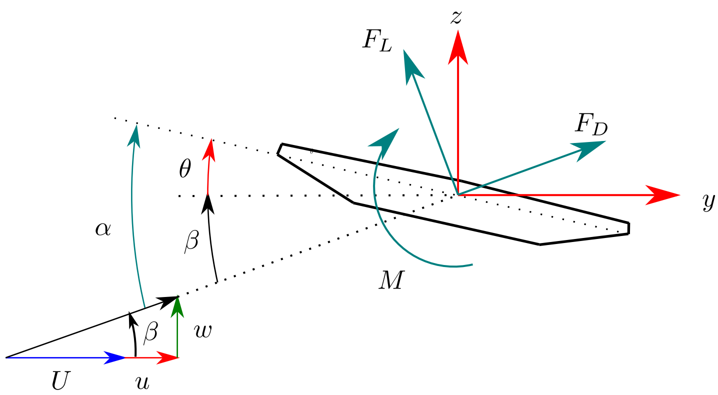

Figure 2: Sign conventions for forces (lift F_L, drag F_D, moment M), displacements (lateral y, vertical z, rotation θ), and wind velocity (turbulent vertical speed w and horizontal u)

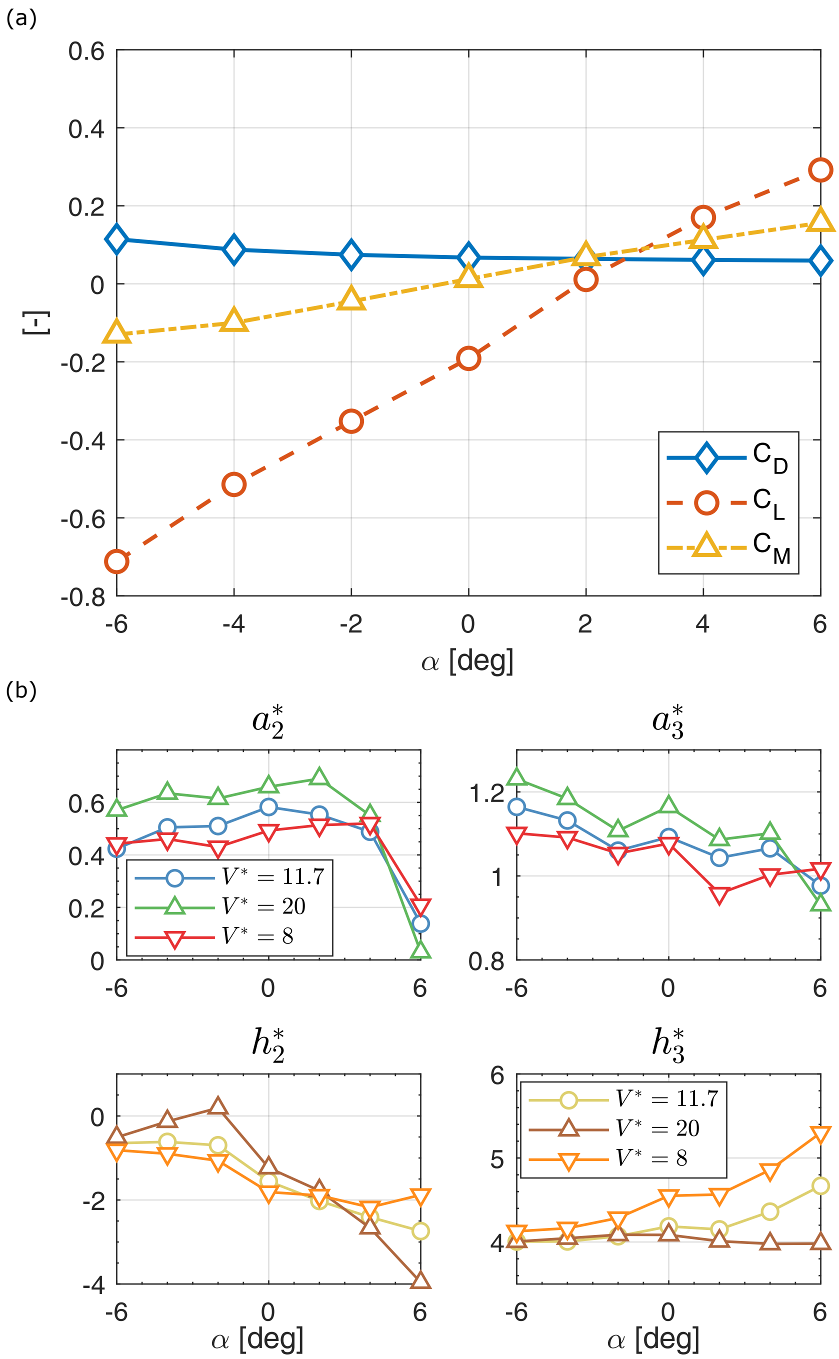

Figure 3: a) Stationary aerodynamic coefficients; b) torsional flutter derivatives a_2^*, a_3^*, h_2^*, h_3^*, as function of the angle of attack at $V^* = [8, 11.7, 20]$

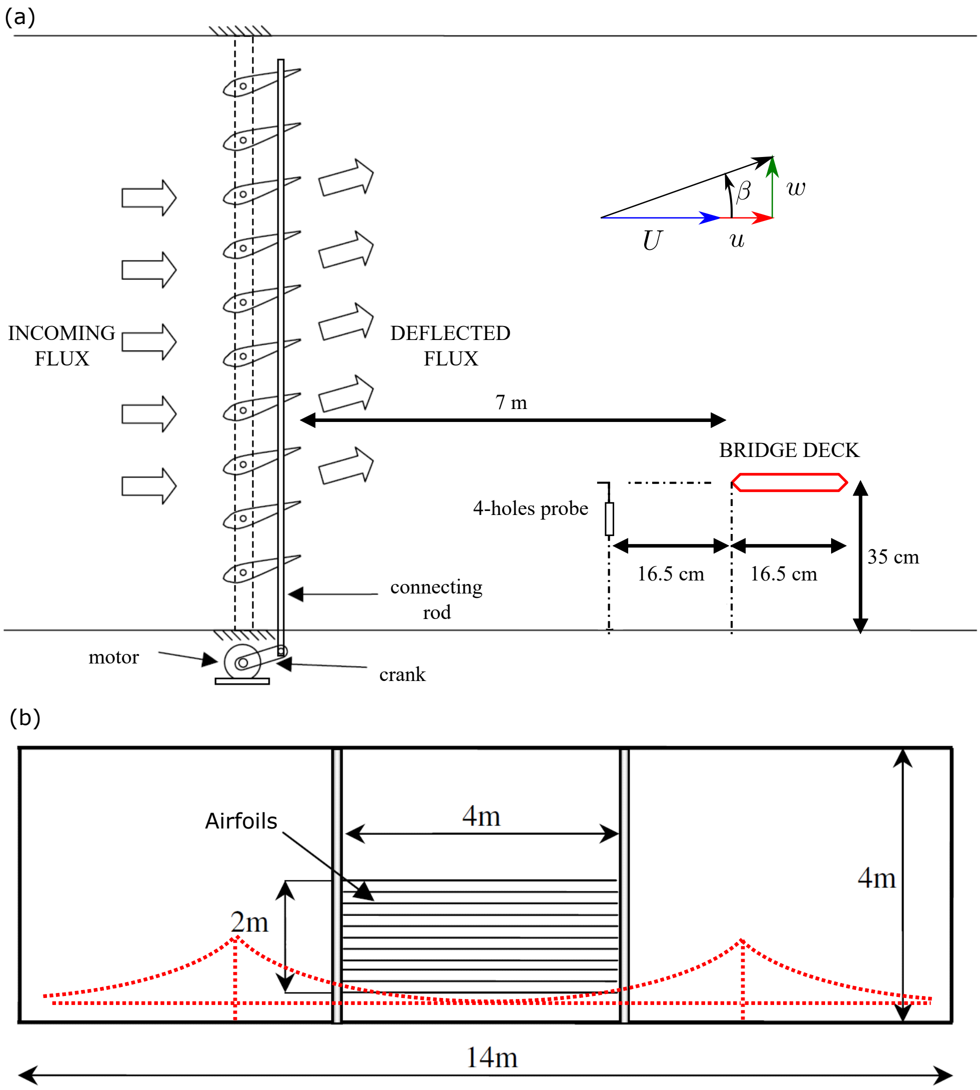

Figure 4: Active turbulence generator: a) side view; b) frontal view

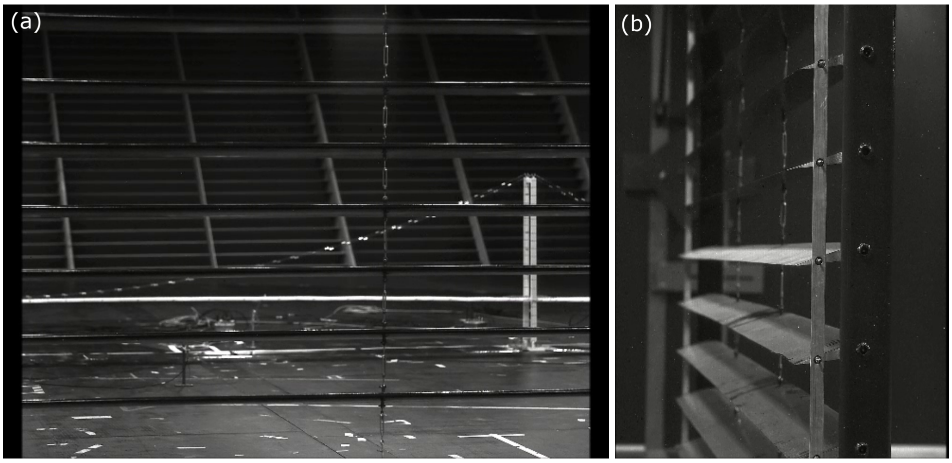

Figure 5: Pictures of the experimental setup. a) active turbulence generator with view of the bridge model in the background; b) details of the airfoils

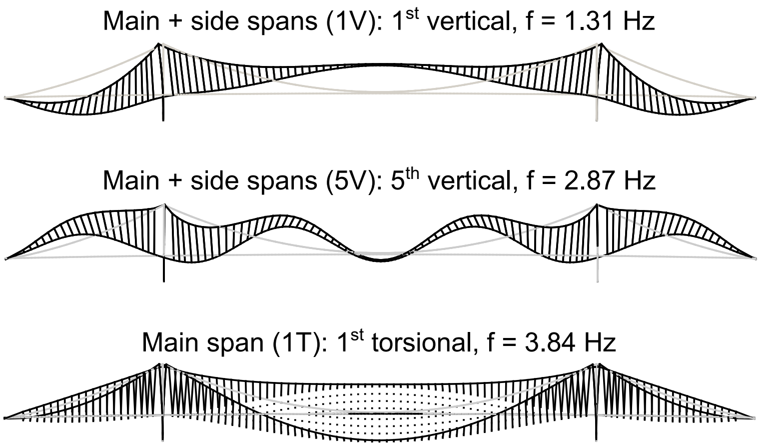

Figure 6: Modal shapes of the first and fifth vertical bending modes (1V and 5V) and of the first torsional mode (1T). f structural modal frequency

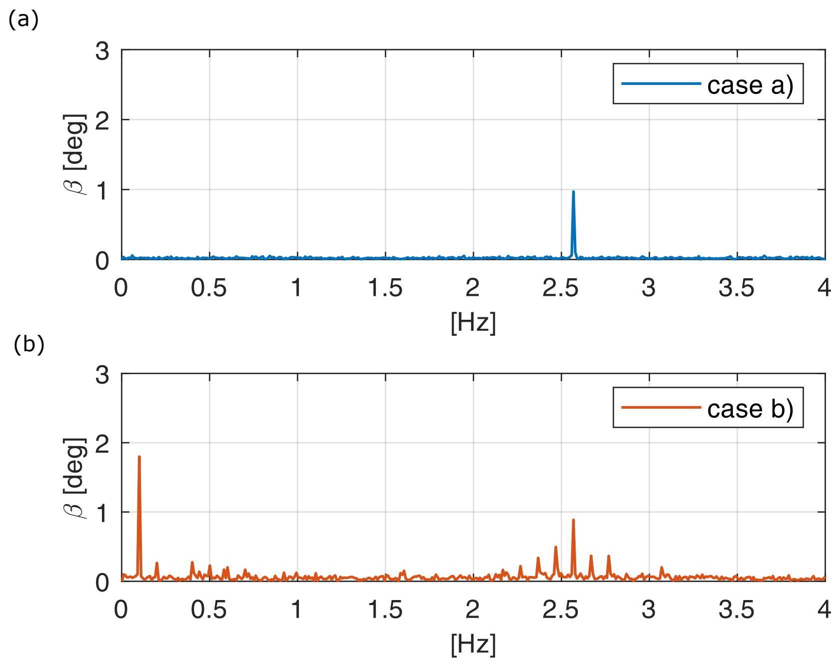

Figure 7: Incoming turbulent wind angle β for Case a) and Case b)

(a)

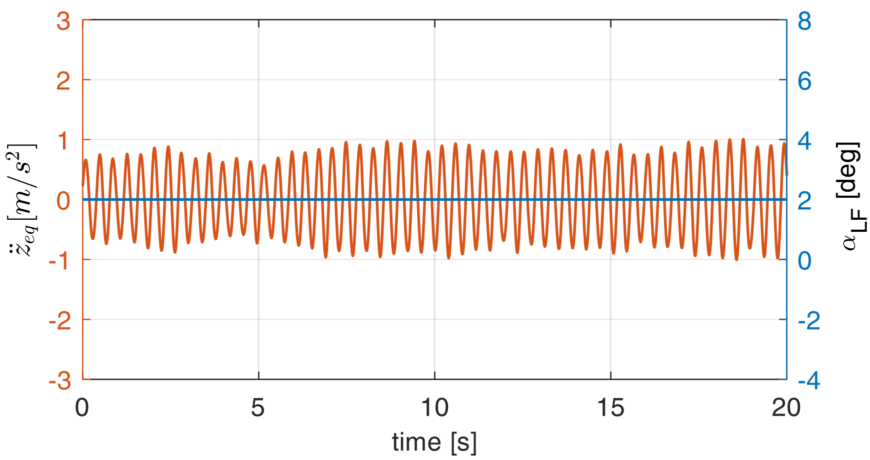

(b)

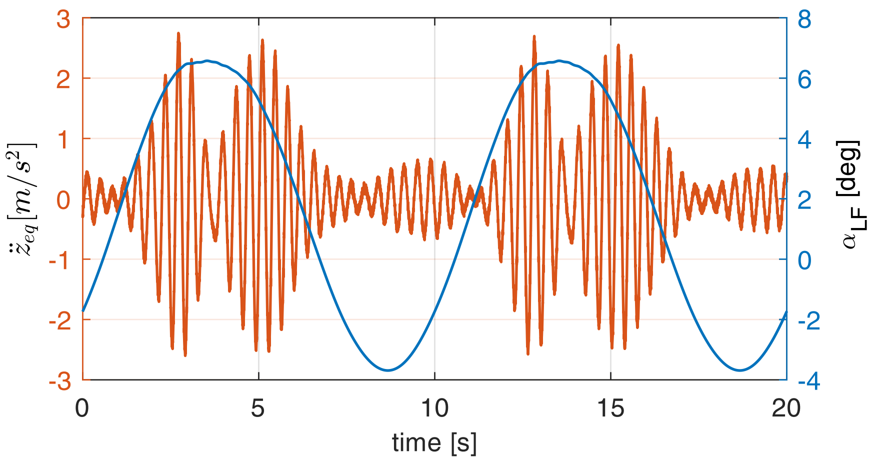

Figure 8: Comparison between torsional response in Case a) and in Case b): mid-span equivalent torsional accelerations at deck edge (red line, left y-axis) and LF angle of attack (blue line, right y-axis)

(a)

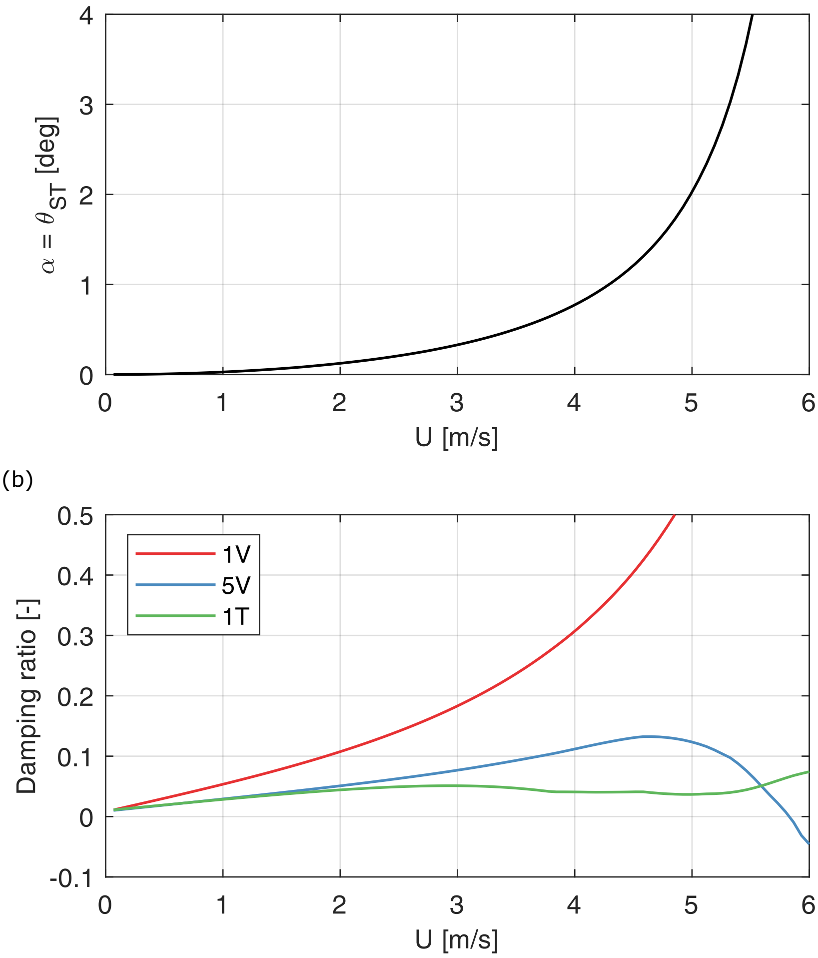

Figure 9: (a) static deck rotation at mid-span as a function of the incoming wind speed; (b) trend of the modal damping ratios as a function of the incoming wind speed for the considered modes (1V, 5V, 1T)

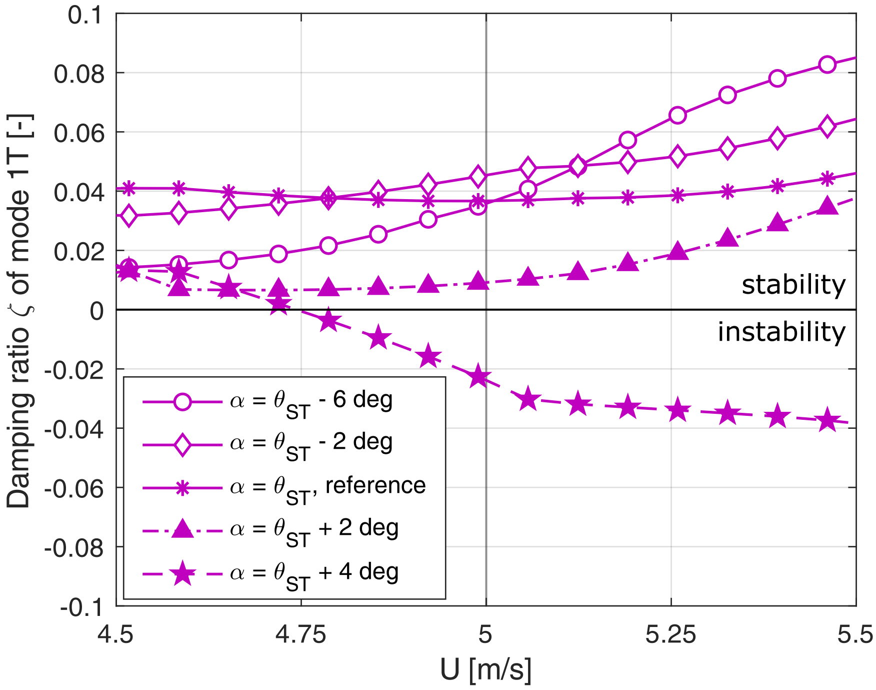

Figure 10: Trend of the modal damping ratio of mode "1T" as a function of the incoming wind speed, for different mean angles of attack α ranging from $\theta_{ST} - 6$ deg to $\theta_{ST} + 4$ deg

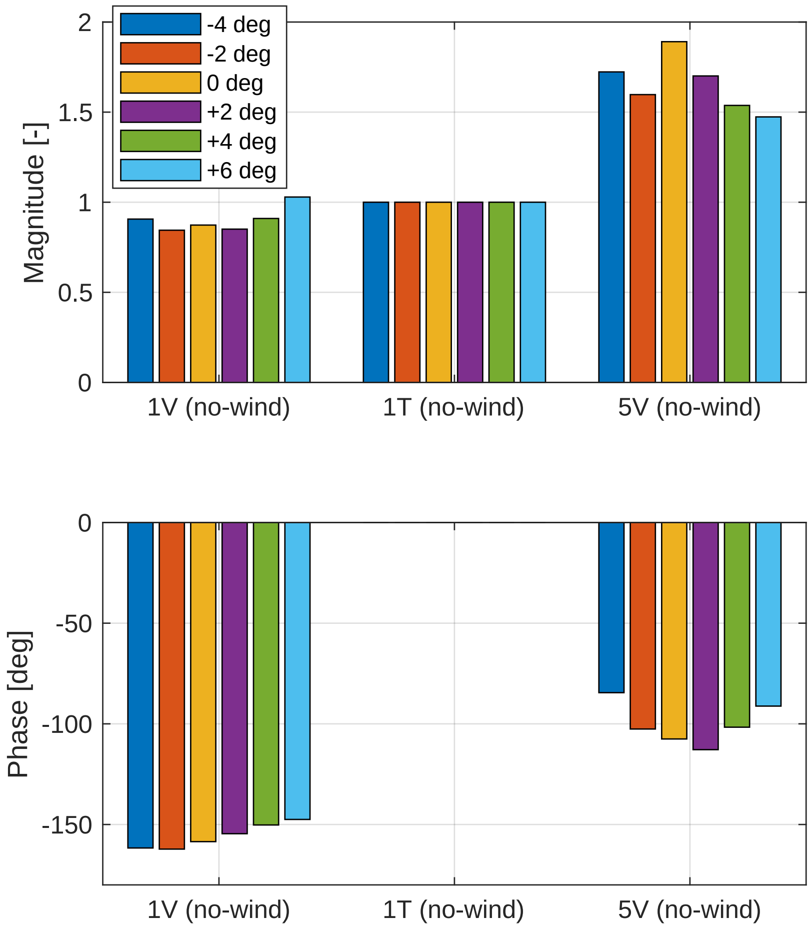

Figure 11: Magnitude and phase of the eigenvector of the mode "1T" at 5 m/s, for different mean angles of attack ranging from -4 to +6 deg

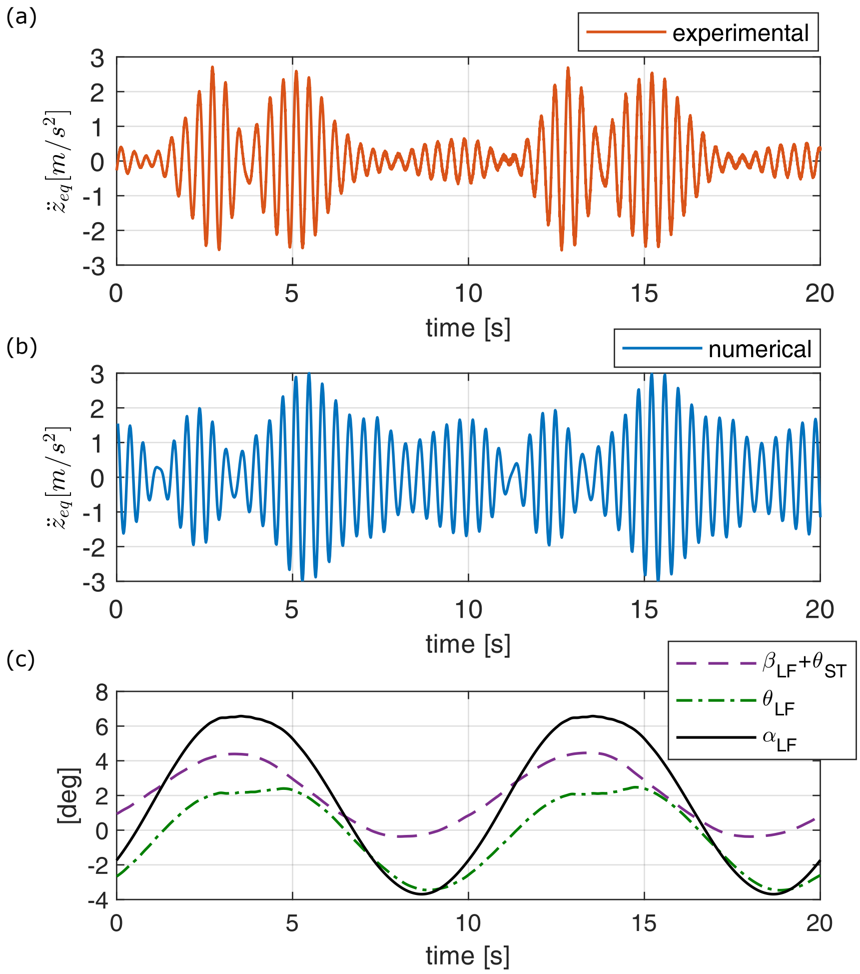

Figure 12: (a) and (b) Comparison of numerical and experimental torsional accelerations, in terms of equivalent torsional accelerations at deck edge $\ddot{z}_{eq}$. (c) Experimental LF angles: deck rotation θ_{LF}, wind angle β_{LF}, and total angle of attack $\alpha_{LF} = \theta_{LF} + \beta_{LF} + \theta_{ST}$.

References

Argentini, T., Diana, G., Rocchi, D., Somaschini, C., 2016. A case-study of double multi-modal bridge flutter: Experimental result and numerical analysis. Journal of Wind Engineering and Industrial Aerodynamics 151, 25–36. doi:10.1016/j.jweia.2016.01.004.

Argentini, T., Pagani, A., Rocchi, D., Zasso, A., 2014. Monte Carlo analysis of total damping and flutter speed of a long span bridge: Effects of structural and aerodynamic uncertainties. Journal of Wind Engineering and Industrial Aerodynamics 128, 90–104. doi:10.1016/j.jweia.2014.02.010.

Bocciolone, M., Cheli, F., Curami, A., Zasso, A., 1992. Wind measurements on the Humber bridge and numerical simulations. Journal of Wind Engineering and Industrial Aerodynamics 42, 1393–1404. doi:10.1016/0167-6105(92)90147-3.

Carassale, L., Wu, T., Kareem, A., 2014. Nonlinear aerodynamic and aeroelastic analysis of bridges: Frequency domain approach. Journal of Engineering Mechanics 140, 04014051. doi:10.1061/(ASCE)EM.1943-7889.0000737.

Chen, X., Kareem, A., 2001. Nonlinear response analysis of long-span bridges under turbulent winds. Journal of Wind Engineering and Industrial Aerodynamics 89, 1335–1350. doi:10.1016/S0167-6105(01)00147-7.

Cheynet, E., Jakobsen, J., Snæbjörnsson, J., Mann, J., Courtney, M., Lea, G., Svardal, B., 2017a. Measurements of surface-layer turbulence in awide norwegian fjord using synchronized long-range doppler wind lidars. Remote Sensing 9, 977. doi:10.3390/rs9100977.

Cheynet, E., Jakobsen, J., Snæbjörnsson, J., Reuder, J., Kumer, V., Svardal, B., 2017b. Assessing the potential of a commercial pulsed lidar for wind characterisation at a bridge site. Journal of Wind Engineering and Industrial Aerodynamics 161, 17–26. doi:10.1016/j.jweia.2016.12.002.

Diana, G., Bruni, S., Rocchi, D., 2005. A numerical and experimental investigation on aerodynamic non linearities in bridge response to turbulent wind., in: EACWE 2005 - 4th European and African Conference on Wind Engineering., pp. 86–87.

Diana, G., Falco, M., Bruni, S., Cigada, A., Larose, G., Darnsgaard, A., Collina, A., 1995. Comparisons between wind tunnel tests on a full aeroelastic model of the proposed bridge over stretto di messina and numerical results. Journal of Wind Engineering and Industrial Aerodynamics 54-55, 101–113. doi:10.1016/0167-6105(94)00034-B.

Diana, G., Resta, F., Rocchi, D., 2008. A new numerical approach to reproduce bridge aerodynamic non-linearities in time domain. Journal of Wind Engineering and Industrial Aerodynamics 96, 1871–1884. doi:10.1016/j.jweia.2008.02.052.

Diana, G., Resta, F., Zasso, A., Belloli, M., Rocchi, D., 2004. Forced motion and free motion aeroelastic tests on a new concept dynamometric section model of the messina suspension bridge. Journal of Wind Engineering and Industrial Aerodynamics 92, 441–462. doi:10.1016/j.jweia.2004.01.005.

Diana, G., Rocchi, D., Argentini, T., 2013a. An experimental validation of a band superposition model of the aerodynamic forces acting on multi-box deck sections. Journal of Wind Engineering & Industrial Aerodynamics 113, 40–58. doi:10.1016/j.jweia.2012.12.005.

Diana, G., Rocchi, D., Argentini, T., Muggiasca, S., 2010. Aerodynamic instability of a bridge deck section model: Linear and nonlinear approach to force modeling. Journal of Wind Engineering and Industrial Aerodynamics 98, 363–374. doi:10.1016/j.jweia.2010.01.003.

Diana, G., Stoyanoff, S., AAS-JAKOBSEN, K., Allsop, A., ANDERSEN, M., Argentini, T., Cid Montoya, M., HERNÁNDEZ, S., Jurado, J.Á., Katsuchi, H., KAVRAKOV, I., Kim, H.K., Larose, G., Larsen, A., Morgenthal, G., Øiseth, O., Omarini, S., Rocchi, D., Svendsen, M., Wu, T., 2019a. IABSE Task Group 3.1

Benchmark Results. Part 1: Numerical analysis of a Two-Degree-of-Freedom Bridge Deck Section Based on Analytical Aerodynamics. Structural Engineering International doi:10.1080/10168664.2019.1661331.

Diana, G., Stoyanoff, S., AAS-JAKOBSEN, K., Allsop, A., ANDERSEN, M., Argentini, T., Cid Montoya, M., HERNÁNDEZ, S., Jurado, J.Á., Katsuchi, H., KAVRAKOV, I., Kim, H.K., Larose, G., Larsen, A., Morgenthal, G., Øiseth, O., Omarini, S., Rocchi, D., Svendsen, M., Wu, T., 2019b. IABSE Task Group 3.1 Benchmark Results. Part 2: Numerical analysis of a Three-Degree-of-Freedom Bridge Deck Section Based on Experimental Aerodynamics. Structural Engineering International doi:10.1080/10168664.2019.1639480.

Diana, G., Yamasaki, Y., Larsen, A., Rocchi, D., Giappino, S., Argentini, T., Pagani, A., Villani, M., Somaschini, C., Portentoso, M., 2013b. Construction stages of the long span suspension izmit bay bridge: wind tunnel test assessment. Journal of Wind Engineering & Industrial Aerodynamics 123, 300–310. doi:10.1016/j.jweia.2013.09.006.

Fenerci, A., Øiseth, O., 2018. Strong wind characteristics and dynamic response of a long-span suspension bridge during a storm. Journal of Wind Engineering and Industrial Aerodynamics 172, 116 – 138. doi:10.1016/j.jweia.2017.10.030.

Hui, M., Larsen, A., Xiang, H., 2009. Wind turbulence characteristics study at the stonecutters bridge site: Part i-mean wind and turbulence intensities. Journal of Wind Engineering and Industrial Aerodynamics 97, 22–36. doi:10.1016/j.jweia.2008.11.002.

Ma, T., Zhao, L., Cao, S., Ge, Y., Miyagi, H., 2013. Investigations of aerodynamic effects on streamlined box girder using two-dimensional actively-controlled oncoming flow. Journal of Wind Engineering and Industrial Aerodynamics 122, 118–129. doi:10.1016/j.jweia.2013.07.011.

Mikkelsen, T., Sjöholm, M., Angelou, N., Mann, J., 2017. 3d WindScanner lidar measurements of wind and turbulence around wind turbines, buildings and bridges. IOP Conference Series: Materials Science and Engineering 276, 012004. doi:10.1088/1757-899x/276/1/012004.

Wu, T., Kareem, A., 2014. Simulation of nonlinear bridge aerodynamics: A sparse third-order volterra model. Journal of Sound and Vibration 333, 178 – 188. doi:https://doi.org/10.1016/j.jsv.2013.09.003.

Zasso, A., 1996. Flutter derivatives: advantages of a new representation convention. Journal of Wind Engineering and Industrial Aerodynamics 60, 35–47. doi:10.1016/0167-6105(96)00022-0.